Iranian Journal of Numerical Analysis and Optimization
Vol. 16, No. 1, 2026, pp 188–219
https://doi.org/10.22067/ijnao.2025.94641.1689
https://ijnao.um.ac.ir/

Research Article

Transdermal drug delivery via a hollow microneedle considering the skin's mechanical properties: Analytical and numerical study

E. Azhdari* and A. Emami

Abstract

Hollow microneedles have a significant impact on transdermal drug delivery by overcoming the stratum corneum layer of the skin and delivering drugs directly to living skin tissues. In this paper, using a mathematical model, the diffusion of nanocarriers, free drugs, and bound drugs in the microneedle channel, different skin layers, and the bloodstream is described. The mechanical properties of the skin, which affect drug delivery due to the elasticity and elastin present in the dermis of the skin, are considered. The qualitative behavior of the model is studied using energy estimation. The well-posedness of the fully coupled system is examined. Numerical simulations are used to study the model's numerical behavior and sensitivity analysis.

AMS subject classifications (2020): Primary 92B99; Secondary 65M12.

*Corresponding author

Received 26 July 2025; revised 9 October 2025; accepted 18 October 2025

Ebrahim Azhdari
Department of Mathematics and Computer Science, Faculty of Basic Sciences, Salman Farsi University of Kazerun, Kazerun, Iran. e-mail: e.azhdari@kazerunsfu.ac.ir

Aram Emami
Department of Mathematics and Computer Science, Faculty of Basic Sciences, Salman Farsi University of Kazerun, Kazerun, Iran. e-mail: emami@kazerunsfu.ac.ir

How to cite this article
Azhdari, E. and Emami, A., Transdermal drug delivery via a hollow microneedle considering the skin's mechanical properties: Analytical and numerical study. *Iran. J. Numer. Anal. Optim.*, 2026; 16(1): 188-219. https://doi.org/10.22067/ijnao.2025.94641.1689

Keywords: Mathematical model; Numerical simulation; Viscoelastic properties; Energy estimate; Hollow microneedles.

1 Introduction

The transdermal drug delivery system has emerged as a powerful, acceptable, and general approach for new drug delivery systems [27]. It has gained great interest in practice due to many advantages such as less invasiveness, ease of application, and so on [19, 32]. A drug applied to the skin's surface must penetrate the stratum corneum (SC) and viable epidermis (VE) in order to reach the blood (BL) vessel-containing papillary dermis (PD), which is determined by the anatomical makeup of the skin. The rest of the drug may enter the lymphatic system or penetrate into the reticular dermis (RD). The topmost layer of the skin, known as the SC, serves as a barrier to protect the skin and stops additional drug penetration because its cells are made up of densely packed, flat, dead keratinocytes without nuclei [28]. This problem doubles the importance of dermal drug delivery by new methods.

To overcome this issue, hollow microneedles (MNs) are used. In general, MNs are divided into five categories, namely solid, hollow, coated, dissolving, and swellable MNs [7, 20, 34]. Hollow MNs contain a channel (CH). After passing through the SC, the MN delivers the drug directly to the underlying layers with the help of the CH, as shown in [7]. For the treatment to be effective, instead of freely transporting the drug to the desired sites, the drug is placed in nanocarriers and the nanocarriers are transported to the desired site through the CH [17]. This prevents the drug molecules from being quickly destroyed by the body.

The dynamic properties of skin tissue, which vary among patients, can affect transdermal drug delivery [18, 29]. It is challenging to isolate these factors experimentally alone. Mathematical modeling can be of great help. Many mathematical models have been studied in the field of transdermal drug delivery [2, 3, 5, 6, 22]. Azhdari and Emami [3] have simulated transdermal drug delivery using polymeric MNs. The effect of MN swelling in the skin on drug delivery has been investigated and studied numerically and analytically. A model explored for drug delivery through hollow MNs was examined by Benbrook and Zhan [5], focusing on the influence of various characteristics of hollow MNs, nanocarriers, clinical environments, and environmental variables . The model presented by Zhan et al. does not address the mechanical properties of the skin, which are influenced by a protein called elastin, which is found in the dermis layer of the skin and has elasticity and stretch properties. In this paper, we study these important properties and show their effect on drug delivery.

The summary of this paper is as follows: In section 2, the anatomy of the skin is discussed. The mathematical model of the problem and the initial and boundary conditions, as well as the viscoelastic effect are presented in section 3. In section 4, the qualitative behavior of the model, using energy estimation, and the well-posedness of the fully coupled system are discussed. Numerical results, numerical simulations, numerical error analysis, and convergence study are presented in section 5. Finally, in section 6, conclusions are presented.

2 The anatomy of the skin

The skin is the covering and protective part of the body, which in addition to having a significant impact on our appearance, also indicates our internal health [21]. The skin is composed of three main layers (Figure 1a), each of which includes a sublayer and appendages that have their own functions and play a role in maintaining the overall structure of the skin [1]. These layers of the skin, from surface to depth, include: epidermis, dermis, and hypodermis. In the case of the epidermis, it is mostly composed of dead cells, and the hypodermis plays a major role in warming the body. The dermis is the second layer of skin located below the epidermis. The dermis of the skin is divided into two areas: one is the PD, and the other is the RD [30]. This layer is composed of connective tissue and contains a large amount of nervous tissue and blood vessels. When it comes to thickness, the dermis is significantly thicker than the epidermis and is responsible for the skin's strength and elasticity. The geometry of the model is shown in Figure 1b. According to this figure, to make sense, we indicate the domains as follows: SC (Ω_s), MN (Ω_m), CH (Ω_c), VE (Ω_e), PD and BL (Ω_p), and RD (Ω_r). Also, $15\mu m$ for SC, $100\mu m$ for VE, $350\mu m$ for PD, and $800\mu m$ for RD are the actual skin layer thickness values that the model is based on. Also, the length of the MN is $250\mu m$ and the width of the CH is $30\mu m$. The cylindrical CH is located in the center of the MN.

3 Mathematical model

The model includes equations that describe the transport of infusate, interstitial fluid, and drug inside the MN CH, skin tissues, and circulatory system. The notations have been included in Table 1 to facilitate the reading of the parameters.

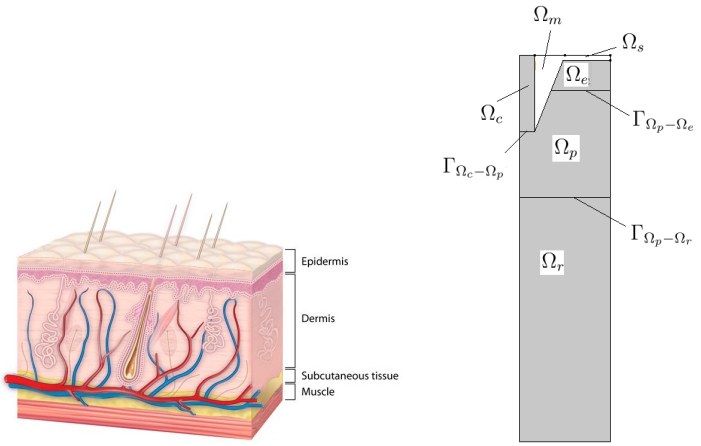

(a) The layers of the skin include: epidermis, dermis, and hypodermis.

(b) The geometry of the model: SC (Ω_s), MN (Ω_m), CH (Ω_c), VE (Ω_e), PD and BL (Ω_p) and RD (Ω_r).

Figure 1: The anatomy of the skin and geometry of the model.

3.1 Fluid transfer model

The fluid inside the MN CH and skin tissues such as VE, PD, and RD, which act as a porous medium, are described with the help of the continuity equation and the moment conservation equation as follows:

$$\nabla \cdot \mathbf{v} = 0, \tag{1}$$

$$\rho \frac{\partial \mathbf{v}}{\partial t} + \rho(\mathbf{v} \cdot \nabla \mathbf{v}) = -\nabla p + \mu \nabla^2 \mathbf{v}, \tag{2}$$

where $\mathbf{v}$ is the velocity, p is the pressure, ρ is the density, and μ is the viscosity.

3.2 Drug delivery model

In this section, a mathematical model for different types of drugs, which are delivered in the form of nanocarriers, released drugs (free drugs), and encapsulated drugs (bound drugs), is presented. The drug is first introduced into the skin tissue in the form of nanocarrier capsules through the

Table 1: Parameter notation and description.

Parameter Notation	Parameter Description
n	Nanocarrier
f	Free drugs
b	Bound drugs
MN (Ω_m)	Microneedle
$e\ VE$ (Ω_e)	Viable epidermis
$c\ SC$ (Ω_s)	Stratum corneum
$p\ PD$ (Ω_p)	Papillary dermis
$r\ RD$ (Ω_r)	Reticular dermis
$c\ CH$ (Ω_c)	Channel
$C_{i,j}$	Concentration of $i = n, f, b$ in Ω_j $j = c, e, p, r, bl$
$D_{i,j}$	Diffusion coefficient of $i = n, f$ in Ω_j $j = e, c, p, r, bl$
$k_{d,i}$	Physical degradation rate of free drug in Ω_j $j = c, e, p, r$
$k_{rel,i}$	Drug release rate in Ω_j $j = e, p, r, bl$
k_{pb}	Drug association rate with protein
k_{pu}	Drug dissociation rate from protein
$k_{clr,i}$	Rate of plasma clearance of $i = n, f$
R_{ly}	Rate of fluid exchange between the PD and lymph
k_{Ex}	Constant dependent
R_{bl}	Rate of fluid exchange
σ_f	Osmotic reflection coefficient of drug
E_1	Stiffness coefficient of the single spring
E_2	Stiffness coefficient of the spring
η	Stiffness coefficient of the dashpot
D_v	Viscoelastic diffusion coefficient
σ	Stress generated by the skin
$\mathbf{v}$	Velocity
p	Pressure
ρ	Density
μ	Viscosity

MN CH. After contact with the skin tissues, the nanocarriers begin to release the drug, and the remaining nanocarriers and released drugs are transported to the adjacent tissues, which depends on how far the MN is inserted into the skin. In this paper, we assume that the tip of the MN passes through the SC and VE and is located in the PD. Nanocarriers and free drugs are subject to elimination in all layers of the skin corresponding to the skin tissues due to biological and physical reactions. In particular, some of the nanocarriers and free drugs in the PD layer may enter the circulatory and lymphatic systems. The transfer of nanocarriers and free drugs within the MN CH, skin layers and bloodstream, determined through the convection, diffusion, degradation and release equations, is expressed as follows:

$$\frac{\partial C_{n,c}}{\partial t} = \nabla \cdot (D_{n,c} \nabla C_{n,c}) - \nabla \cdot (\mathbf{v} C_{n,c}),\ in\ \Omega_c \times (0, T], \tag{3}$$

$$\frac{\partial C_{f,c}}{\partial t} = \nabla \cdot (D_{f,c} \nabla C_{f,c}) - \nabla \cdot (\mathbf{v} C_{f,c}) - k_{d,c} C_{f,c}, \ in\ \Omega_c \times (0,T], \tag{4}$$

$$\frac{\partial C_{n,e}}{\partial t} = \nabla \cdot (D_{n,e} \nabla C_{n,e}) - \nabla \cdot (\mathbf{v} C_{n,e}) - k_{rel,e} C_{n,e}, \ in\ \Omega_e \times (0,T], \tag{5}$$

$$\frac{\partial C_{f,e}}{\partial t} = \nabla \cdot (D_{f,e} \nabla C_{f,e}) - \nabla \cdot (\mathbf{v} C_{f,e}) + k_{rel,e} C_{n,e} - k_{d,e} C_{f,e}, \quad in\ \Omega_e \times (0,T], \tag{6}$$

$$\frac{\partial C_{n,p}}{\partial t} = \nabla \cdot (D_{n,p} \nabla C_{n,p}) - \nabla \cdot (\mathbf{v} C_{n,p}) - R_{ly} C_{n,p} - k_{rel,p} C_{n,p}, \quad in\ \Omega_p \times (0,T], \tag{7}$$

$$\frac{\partial C_{f,p}}{\partial t} = \nabla \cdot (D_{f,p} \nabla C_{f,p}) - \nabla \cdot (\mathbf{v} C_{f,p}) + k_{rel,p} C_{n,p} - k_{d,p} C_{f,p} - R_{ly} C_{f,p} - k_{pb} C_{f,p} + k_{pu} C_{b,p} - Ex[C_{f,p}, C_{f,bl}], \ in\ \Omega_p \times (0,T], \tag{8}$$

$$\frac{dC_{b,p}}{dt} = k_{pb} C_{f,p} - k_{pu} C_{b,p}, \ in\ \Omega_p \times (0,T], \tag{9}$$

$$\frac{\partial C_{n,r}}{\partial t} = \nabla \cdot (D_{n,r} \nabla C_{n,r}) - \nabla \cdot (\mathbf{v} C_{n,r}) - k_{rel,r} C_{n,r}, \ in\ \Omega_r \times (0,T], \tag{10}$$

$$\frac{\partial C_{f,r}}{\partial t} = \nabla \cdot (D_{f,r} \nabla C_{f,r}) - \nabla \cdot (\mathbf{v} C_{f,r}) + k_{rel,r} C_{n,r} - k_{d,r} C_{f,r} \quad in\ \Omega_r \times (0,T], \tag{11}$$

$$\frac{dC_{n,bl}}{dt} = -k_{rel,bl} C_{n,bl} - k_{clr,n} C_{n,bl}, \ in\ \Omega_p \times (0,T], \tag{12}$$

$$\frac{dC_{f,bl}}{dt} = k_{rel,bl} C_{n,bl} - (k_{pb} C_{f,bl} - k_{pu} C_{b,bl}) - k_{clr,f} C_{f,bl} + Ex[C_{f,p}, C_{f,bl}] \quad in\ \Omega_p \times (0,T], \tag{13}$$

$$\frac{dC_{b,bl}}{dt} = k_{pb}C_{f,bl} - k_{pu}C_{b,bl},\ in\ \Omega_p \times (0,T], \tag{14}$$

where $C_{i,j}$ are nanocarrier concentration, free drugs concentration and bound drugs concentration in CH, VE, PD, RD, BL, for $i = n, f, b$ and $j = c, e, p, r, bl$, respectively, $D_{i,j}$ are the diffusion coefficient of nanocarrier and free drugs in CH, VE, PD, RD, for $i = n, f$ and $j = c, e, p, r$, respectively, $k_{d,i}$ are the physical degradation rate of free drug in CH, VE, PD, RD, for $i = c, e, p, r$, respectively, $k_{rel,i}$ are the drug release rate in VE, PD, RD, BL for $i = e, p, r, bl$, respectively, R_{ly} is the rate of fluid exchange between the PD and lymph, k_{pb} is the drug association rate with protein, k_{pu} is the drug dissociation rate from protein, and $k_{clr,n}$ and $k_{clr,f}$ are the plasma clearance rate.

In (8) and (13), the free drugs exchange rate between the PD and BL is defined as

$$Ex[C_{f,p}, C_{f,bl}] = k_{Ex}(C_{f,p} - C_{f,bl}) - R_{bl}(1 - \sigma_f)C_{f,bl}, \tag{15}$$

where k_{Ex} is a constant dependent on the vascular permeability of nanocarriers and capillary surface area per unit of tissue volume, R_{bl} is the rate of fluid exchange between the PD and the blood, and σ_f is the osmotic reflection coefficient of drug.

The following can be mentioned as a biological implication of the equations. Diffusion and convection with flow of interstitial fluid are required in VE, while in MN, convection, infusion, and diffusion are required to transport drug nanocarriers. In PD, transport of nanocarriers is dependent not only on diffusion, convection and release of the drug but also determined by exchange between the tissue and circulatory systems, whereas in RD, transport is mediated by convection, diffusion, and local release of the drug. Exchange between BL and PD, local release of the drug and plasma clearance all affect the blood concentration of the drug nanocarriers.

3.3 Viscoelastic effects

Elastin is a protein found naturally in the dermis of the skin and has elasticity and stretch properties. This protein allows the skin to return to its original shape after being stretched. This phenomenon causes the skin to become resistant to the drug's entry into the PD through the MN CH. Therefore, to describe the viscoelastic behavior of the skin, it is necessary to add the term $\nabla.(D_v \nabla\sigma)$ to the right-hand side of (7) and (8). Keeping the sign used by Ferreira et al. [13], σ denotes the stress generated by the skin and D_v is called the viscoelastic diffusion coefficient. Therefore, (7) and (8) change as follows after this explanation:

$$\frac{\partial C_{n,p}}{\partial t} = \nabla \cdot (D_{n,p}\nabla C_{n,p}) + \nabla.(D_v \nabla \sigma) - \nabla \cdot (\mathbf{v} C_{n,p}) - R_{ly} C_{n,p} \\ -k_{rel,p} C_{n,p}, \tag{16}$$

$$\frac{\partial C_{f,p}}{\partial t} = \nabla \cdot (D_{f,p}\nabla C_{f,p}) + \nabla.(D_v \nabla \sigma) - \nabla \cdot (\mathbf{v} C_{f,p}) + k_{rel,p} C_{n,p} - k_{d,p} C_{f,p} \\ -R_{ly} C_{f,p} - k_{pb} C_{f,p} + k_{pu} C_{b,p} - Ex[C_{f,p}, C_{f,bl}]. \tag{17}$$

Many viscoelastic models obtained under different experimental conditions are presented here [24, 31]. In what follows, we present one of the simplest models, also known as the Zener model, which is linear [4, 26]. The model presented is used to describe the viscoelastic behavior of skin due to the presence of elastin in the dermis layer. The delay times used in this model are consistent with those predicted for viscoelastic behavior in living tissues [25]. The system is made up of a spring in parallel with a spring-dashpot in series, and the connection between stress and strain is depicted as follows:

$$\frac{d\sigma}{E_2 \times dt} + \frac{\sigma}{\eta} = (1 + \frac{E_1}{E_2}) \times \frac{d\epsilon}{dt} + \frac{E_1}{\eta} \times \epsilon, \tag{18}$$

where ϵ is the strain created by the nanocarrier and drug molecules. E_1 represents the sole spring's stiffness and E_2 and η represent the spring-dashpot pair's stiffness and damping factor, respectively.

To demonstrate that the skin prevents the drug from entering the PD, the terms on the right side of (18) must be multiplied by a negative sign, meaning that σ and ϵ have opposite signs.

As stated in [4, 12], in (18), we assume the relationship between strain and the concentration of drug and nanocarriers as the following linear relationship:

$$\epsilon = f(C_i), \qquad i = n, p \ and \ f, p. \tag{19}$$

The diffusion of solute through viscoelastic materials does not obey the Fick Law. This is because, in biological terms, for example, the concentration of the solvent may change the physical structure of the tissue (e.g., cartilage, hydrogel, or cell-filled matrix). The viscoelastic matrix is in opposition to the Brownian motion of the molecules, which can be measured by the stress reaction to the strain. Several authors have proposed a general model in which the flux is due to two phenomena: the concentration gradient of a solute and the stress gradient created by the matrix [13, 15]. Therefore, to measure the stress created in (16)–(17), we represent it with

the simplest Zener model that includes both instantaneous elasticity and delayed viscoelasticity. To solve (18), we provide the strain ϵ based on the concentration C_i for $i = n, p$ and $i = f, p$.

Many biological materials are porous, hydrated structures. The concentration of fixed charges on proteoglycans attracts counterions, creating an osmotic pressure difference. Increasing the concentration of C_i for $i = n, p$ and $i = f, p$ ions within the tissue directly leads to volumetric strain and swelling. This relationship is often linear over a range of physiologically relevant concentrations. Mathematically, in the Taylor expansion, if the deviation is small, then the terms with higher orders can be eliminated. So we get a linear relationship between strain and concentration.

3.4 Initial and boundary conditions

The mathematical model describing the MNs with holes inserted into the skin and solved in two dimensions for drug delivery. Throughout the entire computational domain, the initial concentrations of the free and bound drugs are taken to be zero, whereas the nanocarrier concentration in CH is taken to be the starting concentration at the start.

No liquid or drug passes through the wall of the MN cavity. Also, the CH surface is a hard wall and the drug flux is zero. The drug is taken to be zero in the vicinity of the computational domain (Ω_e, Ω_p and Ω_r). Therefore, we have the following boundary condition:

$$D\nabla C \cdot \eta = 0, \tag{20}$$

where η is the exterior unit normal, D represents the diffusion coefficient of free drugs or nanocarriers, and C represents the concentration.

Boundary conditions are applied at the interface boundaries between different layers of the skin, $\Gamma_{\Omega_p-\Omega_e}$ and $\Gamma_{\Omega_p-\Omega_r}$, as well as at the interface boundary between the CH and the skin tissue, $\Gamma_{\Omega_c-\Omega_p}$, for drug and fluid transport are as follows:

$$\begin{cases} D_1\nabla C_1 \cdot \eta_1 = \iota_{1,2}(C_1 - C_2), \\ D_2\nabla C_2 \cdot \eta_2 = -D_1\nabla C_1 \cdot \eta_1, \end{cases} \tag{21}$$

where η_1 and η_2 are the exterior unit normal, D_1 and D_2 are the diffusion coefficient of nanocarriers or free drugs in the domains with an interface boundary, C_1 and C_2 are the concentration in the domains with an interface boundary, and $\iota_{1,2}$ is the mass transfer coefficient of the interfaces.

The MN surface is a hard wall, so the flow velocity at the MN boundary is zero. For the various layer boundaries of the skin, we have assumed that the flow velocity at these boundaries is zero. This indicates that the skin's boundary walls are regarded as rigid, establishing a stationary no-slip boundary condition on the walls. Therefore boundary conditions for the flow velocity in all domains are assumed to be zero, $\mathbf{v} = 0$.

4 Well-posedness

In this section, we use the energy estimate to arrive at the stability of the solution for a finite time interval, from which the existence of the solution also follows. We also show the uniqueness of the solution.

4.1 Energy estimates

In this section, we will discuss an energy estimate that gives us an overview of the qualitative behavior of the problem. First, we solve (18) to get

$$\begin{aligned}\sigma(t) = \sigma(0)e^{-\frac{E_2}{\eta}t} - (E_1+E_2)\epsilon(t) + (E_1+E_2)\epsilon(0)e^{-\frac{E_2}{\eta}t} \\ +\frac{E_2^2}{\eta}\int_0^t \epsilon(s)e^{-\frac{E_2}{\eta}(t-s)}ds.\end{aligned} \tag{22}$$

By Applying (22) in (16) and (17) and considering (19), we get

$$\begin{aligned}\frac{\partial C_{n,p}}{\partial t} = \nabla\cdot(D^*_{n,p}\nabla C_{n,p}) + \frac{D_v E_2^2}{\eta}\int_0^t e^{-\frac{E_2}{\eta}(t-s)}\nabla^2 C_{n,p}ds \\ -\nabla\cdot(\mathbf{v}C_{n,p}) - R_{ly}C_{n,p} - k_{rel,p}C_{n,p},\end{aligned} \tag{23}$$

$$\begin{aligned}\frac{\partial C_{f,p}}{\partial t} = \nabla\cdot(D^*_{f,p}\nabla C_{f,p}) + \frac{D_v E_2^2}{\eta}\int_0^t e^{-\frac{E_2}{\eta}(t-s)}\nabla^2 C_{f,p}ds - \nabla\cdot(\mathbf{v}C_{f,p}) \\ +k_{rel,p}C_{n,p} - k_{d,p}C_{f,p} - R_{ly}C_{f,p} - k_{pb}C_{f,p} \\ +k_{pu}C_{b,p} - Ex[C_{f,p}, C_{f,bl}],\end{aligned} \tag{24}$$

where $D^*_{i,p} = D_{i,p} - D_v(E_1+E_2)$ for $i = n, f$.

Note that the new interface boundary conditions for (23)–(24) are following

$$\begin{cases} (D_1\nabla C_1 + \dfrac{D_v E_2^2}{\eta}\displaystyle\int_0^t e^{-\frac{E_2}{\eta}(t-s)}\nabla C_1 ds)\cdot\eta_1 = \iota_{1,2}(C_1 - C_2), \\ D_2\nabla C_2\cdot\eta_2 = -(D_1\nabla C_1 + \dfrac{D_v E_2^2}{\eta}\displaystyle\int_0^t e^{-\frac{E_2}{\eta}(t-s)}\nabla C_1 ds)\cdot\eta_1. \end{cases} \tag{25}$$

By multiplying (3)–(6), (9)–(14) and (23)–(24) by $\phi_{i,j}$ for $i = n, f, b$ and $j = c, e, p, r, bl$, we obtain

$$\begin{aligned}(\frac{\partial C_{n,c}}{\partial t}, \phi_{n,c}) = &-(D_{n,c}\nabla C_{n,c}, \nabla\phi_{n,c}) + (\mathbf{v}C_{n,c}, \nabla\phi_{n,c}) \\ &+ \int_{\partial\Omega_c} D_{n,c}\nabla C_{n,c}\cdot\phi_{n,c}ds - \int_{\partial\Omega_c}\mathbf{v}C_{n,c}\cdot\phi_{n,c}ds,\end{aligned} \tag{26}$$

$$\begin{aligned}(\frac{\partial C_{f,c}}{\partial t}, \phi_{f,c}) = &-(D_{f,c}\nabla C_{f,c}, \nabla\phi_{f,c}) + (\mathbf{v}C_{f,c}, \nabla\phi_{f,c}) - k_{d,c}(C_{f,c}, \phi_{f,c}) \\ &+ \int_{\partial\Omega_c} D_{f,c}\nabla C_{f,c}\cdot\phi_{f,c}ds - \int_{\partial\Omega_c}\mathbf{v}C_{f,c}\cdot\phi_{f,c}ds,\end{aligned} \tag{27}$$

$$\begin{aligned}(\frac{\partial C_{n,e}}{\partial t}, \phi_{n,e}) = &-(D_{n,e}\nabla C_{n,e}, \nabla\phi_{n,e}) + (\mathbf{v}C_{n,e}, \nabla\phi_{n,e}) - k_{rel,e}(C_{n,e}, \phi_{n,e}) \\ &+ \int_{\partial\Omega_e} D_{n,e}\nabla C_{n,e}\cdot\phi_{n,e}ds - \int_{\partial\Omega_e}\mathbf{v}C_{n,e}\cdot\phi_{n,e}ds,\end{aligned} \tag{28}$$

$$\begin{aligned}(\frac{\partial C_{f,e}}{\partial t}, \phi_{f,e}) = &-(D_{f,e}\nabla C_{f,e}, \nabla\phi_{f,e}) + (\mathbf{v}C_{f,e}, \nabla\phi_{f,e}) + k_{rel,e}(C_{n,e}, \phi_{f,e}) \\ &+ \int_{\partial\Omega_e} D_{f,e}\nabla C_{f,e}\cdot\phi_{f,e}ds \\ &- \int_{\partial\Omega_e}\mathbf{v}C_{f,e}\cdot\phi_{f,e}ds - k_{d,e}(C_{f,e}, \phi_{f,e}),\end{aligned} \tag{29}$$

$$(\frac{dC_{b,p}}{dt}, \phi_{b,p}) = k_{pb}(C_{f,p}, \phi_{b,p}) - k_{pu}(C_{b,p}, \phi_{b,p}), \tag{30}$$

$$(\frac{\partial C_{n,r}}{\partial t},\phi_{n,r}) = -(D_{n,r}\nabla C_{n,r},\nabla\phi_{n,r}) + (\mathbf{v}C_{n,r},\nabla\phi_{n,r}) - k_{rel,r}(C_{n,r},\phi_{n,r}) + \int_{\partial\Omega_r} D_{n,r}\nabla C_{n,r}\cdot\phi_{n,r}ds - \int_{\partial\Omega_r}\mathbf{v}C_{n,r}\cdot\phi_{n,r}ds, \tag{31}$$

$$(\frac{\partial C_{f,r}}{\partial t},\phi_{f,r}) = -(D_{f,r}\nabla C_{f,r},\nabla\phi_{f,r}) + (\mathbf{v}C_{f,r},\nabla\phi_{f,r}) + \int_{\partial\Omega_r} D_{f,r}\nabla C_{f,r}\cdot\phi_{f,r}ds - \int_{\partial\Omega_r}\mathbf{v}C_{f,r}\cdot\phi_{f,r}ds - k_{d,r}(C_{f,r},\phi_{f,r}) + k_{rel,r}(C_{n,r},\phi_{f,r}), \tag{32}$$

$$(\frac{dC_{n,bl}}{dt},\phi_{n,bl}) = -k_{rel,bl}(C_{n,bl},\phi_{n,bl}) - k_{clr,n}(C_{n,bl},\phi_{n,bl}), \tag{33}$$

$$(\frac{dC_{f,bl}}{dt},\phi_{f,bl}) = k_{rel,bl}(C_{n,bl},\phi_{f,bl}) - k_{pb}(C_{f,bl},\phi_{f,bl}) + k_{pu}(C_{b,bl},\phi_{f,bl}) - k_{clr,f}(C_{f,bl},\phi_{f,bl}) + k_{Ex}(C_{f,p},\phi_{f,bl}) - k_{Ex}(C_{f,bl},\phi_{f,bl}) - R_{bl}(1-\sigma_f)(C_{f,bl},\phi_{f,bl}), \tag{34}$$

$$(\frac{dC_{b,bl}}{dt},\phi_{b,bl}) = k_{pb}(C_{f,bl},\phi_{b,bl}) - k_{pu}(C_{b,bl},\phi_{b,bl}), \tag{35}$$

$$(\frac{\partial C_{n,p}}{\partial t},\phi_{n,p}) = -(D^*_{n,p}\nabla C_{n,p},\nabla\phi_{n,p}) + \int_{\partial\Omega_p} D^*_{n,p}\nabla C_{n,p}\cdot\phi_{n,p}ds - \int_{\partial\Omega_p}\mathbf{v}C_{n,p}\cdot\phi_{n,p}ds - k_{rel,p}(C_{n,p},\phi_{n,p}) - R_{ly}(C_{n,p},\phi_{n,p}) - \frac{D_vE_2^2}{\eta}\int_0^t e^{-\frac{E_2}{\eta}(t-s)}(\nabla C_{n,p},\nabla\phi_{n,p})ds + (\mathbf{v}C_{n,p},\nabla\phi_{n,p}) + \frac{D_vE_2^2}{\eta}\int_{\partial\Omega_p}\int_0^t e^{-\frac{E_2}{\eta}(t-s)}(\nabla C_{n,p},\phi_{n,p})d, \tag{36}$$

$$(\frac{\partial C_{f,p}}{\partial t},\phi_{f,p}) = -(D^*_{f,p}\nabla C_{f,p},\nabla\phi_{f,p}) + (\mathbf{v}C_{f,p},\nabla\phi_{f,p}) + k_{pu}(C_{b,p},\phi_{f,p}) - \int_{\partial\Omega_p}\mathbf{v}C_{f,p}\cdot\phi_{f,p}ds + k_{rel,p}(C_{n,p},\phi_{f,p}) - R_{ly}(C_{f,p},\phi_{f,p})$$

$$
\begin{aligned}
&-\frac{D_v E_2^2}{\eta}\int_0^t e^{-\frac{E_2}{\eta}(t-s)}(\nabla C_{f,p},\nabla\phi_{f,p})ds - k_{Ex}(C_{f,p},\phi_{f,p})\\
&+\frac{D_v E_2^2}{\eta}\int_{\partial\Omega_p}\int_0^t e^{-\frac{E_2}{\eta}(t-s)}(\nabla C_{f,p},\phi_{f,p})ds + k_{Ex}(C_{f,bl},\phi_{f,p})\\
&+R_{bl}(1-\sigma_f)(C_{f,bl},\phi_{f,p}) - k_{d,p}(C_{f,p},\phi_{f,p}) - k_{pb}(C_{f,p},\phi_{f,p})\\
&+\int_{\partial\Omega_p} D^*_{f,p}\nabla C_{f,p}\cdot\phi_{f,p}ds.
\end{aligned}
\tag{37}
$$

By taking $\phi_{i,j}=C_{i,j}$ for $i=n,f,b$ and $j=c,e,r,p,bl$, and summing up the equations, and considering the boundary and interface boundary conditions, we obtain

$$
\begin{aligned}
&\frac{1}{2}\frac{d}{dt}\sum_{\substack{i=n,f\\ j=c,p,e,r,bl}}\|C_{i,j}\|^2_{L^2(\Omega_j)} + \frac{1}{2}\frac{d}{dt}\sum_{i=p,bl}\|C_{b,i}\|^2_{L^2(\Omega_p)}\\
&+\sum_{\substack{i=n,f\\ j=c,e,r}} D_{i,j}\|\nabla C_{i,j}\|^2_{[L^2(\Omega_j)]^2} + \sum_{i=n,f} D^*_{i,p}\|\nabla C_{i,p}\|^2_{[L^2(\Omega_p)]^2}\\
&+\sum_{i=c,e,p,r} k_{d,i}\|C_{f,i}\|^2_{L^2(\Omega_i)} + \sum_{i=e,p,r,bl} k_{rel,i}\|C_{n,i}\|^2_{L^2(\Omega_i)}\\
&+\sum_{i=n,f} R_{ly}\|C_{i,p}\|^2_{L^2(\Omega_p)} + \sum_{i=p,bl} k_{pb}\|C_{f,i}\|^2_{L^2(\Omega_p)} + R_{bl}(1-\sigma_f)\|C_{f,bl}\|^2_{L^2(\Omega_p)}\\
&+\sum_{i=n,f} k_{clr,i}\|C_{i,bl}\|^2_{L^2(\Omega_p)} + \sum_{i=p,bl} k_{Ex}\|C_{f,i}\|^2_{L^2(\Omega_p)} + \sum_{i=p,bl} k_{pu}\|C_{b,i}\|^2_{L^2(\Omega_p)}\\
&+\sum_{\substack{i=c,p\\ j=p,e,r\\ k=n,f}} \iota_{i,j}\|[C_{k,i,j}]\|^2_{L^2(\Gamma_{i,j})}\\
&\quad=\sum_{\substack{i=n,f\\ j=c,p,e,r}}\big(\mathbf{v}C_{i,j},\nabla C_{i,j}\big) + 2k_{Ex}\big(C_{f,p},C_{f,bl}\big)\\
&\qquad+R_{bl}(1-\sigma_f)\big(C_{f,bl},C_{f,p}\big) + \sum_{i=p,bl} k_{pb}\big(C_{b,i},C_{f,i}\big)\\
&\qquad+\sum_{i=p,e,r,bl} k_{rel,i}\big(C_{n,i},C_{f,i}\big) + \sum_{i=p,bl} k_{pu}\big(C_{b,i},C_{f,i}\big)\\
&\qquad-\sum_{i=n,f}\frac{D_v E_2^2}{\eta}\int_0^t e^{-\frac{E_2}{\eta}(t-s)}(\nabla C_{i,p}(s),\nabla C_{i,p}(t))ds.
\end{aligned}
\tag{38}
$$

Note that we consider $\sigma(0)$, $C_{n,p}(0)$ and $C_{f,p}(0)$ as constants. In (38), the symbol $[C_{k,i,j}]=(C_{k,i}-C_{k,j})$ represents the exchange of concentrations of nanocarrier and drug at the interface boundary between the two domains. It is shown with this symbol for convenience. Only ordered

pairs of $(c,p),(p,e)$, and (p,r) are permitted in the final term on the left side of (38). It is important to note that in (38), wherever $L^2(\Omega_{bl})$ appears, it means $L^2(\Omega_p)$.

Use Cauchy's inequality with epsilon to get

$$\sum_{\substack{i=n,f\\ j=c,p,e,r}} (\mathbf{v}C_{i,j}, \nabla C_{i,j}) \leq \sum_{\substack{i=n,f\\ j=c,p,e,r}} \big(\frac{1}{4\epsilon_{i,j}^2}\|\mathbf{v}\|_\infty^2 \|C_{i,j}\|^2_{L^2(\Omega_j)} + \epsilon_{i,j}^2 \|\nabla C_{i,j}\|^2_{[L^2(\Omega_j)]^2}\big),$$

$$\sum_{i=p,e,r,bl} k_{rel,i}\big(C_{n,i}, C_{f,i}\big) \leq \sum_{i=p,e,r,bl} \big(\frac{k_{rel,i}}{4\epsilon_{rel,i}^2}\|C_{n,i}\|^2_{L^2(\Omega_i)} + \epsilon_{rel,i}^2 \|C_{f,i}\|^2_{L^2(\Omega_i)}\big),$$

$$\sum_{i=p,bl} k_{pu}\big(C_{b,i}, C_{f,i}\big) \leq \sum_{i=p,bl} \big(\frac{k_{pu}}{4\epsilon_{pu,i}^2}\|C_{b,i}\|^2_{L^2(\Omega_p)} + \epsilon_{pu,i}^2 \|C_{f,i}\|^2_{L^2(\Omega_p)}\big),$$

$$\sum_{i=p,bl} k_{pb}\big(C_{b,i}, C_{f,i}\big) \leq \sum_{i=p,bl} \big(\frac{k_{pb}}{4\epsilon_{pb,i}^2}\|C_{b,i}\|^2_{L^2(\Omega_p)} + \epsilon_{pb,i}^2 \|C_{f,i}\|^2_{L^2(\Omega_p)}\big),$$

$$2k_{Ex}\big(C_{f,p}, C_{f,bl}\big) \leq \frac{k_{Ex}}{2\epsilon_{Ex}^2}\|C_{f,p}\|^2_{L^2(\Omega_p)} + \epsilon_{Ex}^2 \|C_{f,bl}\|^2_{L^2(\Omega_p)},$$

$$R_{bl}(1-\sigma_f)\big(C_{f,bl}, C_{f,p}\big) \leq \frac{R_{bl}(1-\sigma_f)}{4\epsilon_{bl}^2}\|C_{f,p}\|^2_{L^2(\Omega_p)} + \epsilon_{bl}^2 \|C_{f,bl}\|^2_{L^2(\Omega_p)},$$

$$\begin{aligned} &-\sum_{i=n,f} \frac{D_v E_2^2}{\eta}\int_0^t e^{-\frac{E_2}{\eta}(t-s)}(\nabla C_{i,p}(s), \nabla C_{i,p}(t))ds \\ &\quad\leq \sum_{i=n,f}\big(\epsilon_{i,\sigma}^2\|\nabla C_{i,p}(t)\|^2 + \frac{D_v^2 E_2^3}{8\epsilon_{i,\sigma}^2\eta}\int_0^t \|\nabla C_{i,p}(s)\|^2 ds\big). \end{aligned}$$

Multiplying (38) by two and using above inequalities, we obtain

$$\frac{d}{dt}\sum_{\substack{i=n,f\\ j=c,p,e,r,bl}} \|C_{i,j}\|^2_{L^2(\Omega_j)} + \frac{d}{dt}\sum_{i=p,bl}\|C_{b,i}\|^2_{L^2(\Omega_p)} + \sum_{i=n,f} 2R_{ly}\|C_{i,p}\|^2_{L^2(\Omega_p)}$$

$$
\begin{aligned}
&+\sum_{\substack{i=n,f\\ j=c,e,r}} 2\big(D_{i,j}-\epsilon_{i,j}^2-\epsilon_{i,\sigma}^2\big)\|\nabla C_{i,j}\|^2_{[L^2(\Omega_j)]^2}+\sum_{i=e,p,r,bl} 2k_{rel,i}\|C_{n,i}\|^2_{L^2(\Omega_i)}\\
&+\sum_{i=n,f} 2\big(D^*_{i,p}-\epsilon_{i,p}^2-\epsilon_{i,\sigma}^2\big)\|\nabla C_{i,p}\|^2_{[L^2(\Omega_p)]^2}+\sum_{i=c,e,p,r} 2k_{d,i}\|C_{f,i}\|^2_{L^2(\Omega_i)}\\
&+\sum_{i=p,bl} 2k_{pb}\|C_{f,i}\|^2_{L^2(\Omega_p)}+\sum_{i=p,bl} 2k_{pu}\|C_{b,i}\|^2_{L^2(\Omega_p)}\\
&+\sum_{i=n,f} 2k_{clr,i}\|C_{i,bl}\|^2_{L^2(\Omega_p)}+\sum_{i=p,bl} 2k_{Ex}\|C_{f,i}\|^2_{L^2(\Omega_p)}\\
&+2R_{bl}(1-\sigma_f)\|C_{f,bl}\|^2_{L^2(\Omega_p)}+\sum_{\substack{i=c,p\\ j=p,e,r\\ k=n,f}} 2\iota_{i,j}\|[C_{k,i,j}]\|^2_{L^2(\Gamma_{i,j})}\\
&\le \sum_{\substack{i=n,f\\ j=c,p,e,r}} \frac{1}{2\epsilon_{i,j}^2}\|\mathbf{v}\|^2_\infty\|C_{i,j}\|^2_{L^2(\Omega_j)}+\sum_{i=p,e,r,bl}\frac{k_{rel,i}}{2\epsilon^2_{rel,i}}\|C_{n,i}\|^2_{L^2(\Omega_i)}\\
&\quad+\sum_{i=p,e,r,bl} 2\epsilon^2_{rel,i}\|C_{f,i}\|^2_{L^2(\Omega_i)}+\sum_{i=p,bl}\Big(\frac{k_{pu}}{2\epsilon^2_{pu,i}}+\frac{k_{pb}}{2\epsilon^2_{pb,i}}\Big)\|C_{b,i}\|^2_{L^2(\Omega_p)}\\
&\quad+\sum_{i=p,bl} 2(\epsilon^2_{pu,i}+\epsilon^2_{pb,i})\|C_{f,i}\|^2_{L^2(\Omega_p)}+\Big(\frac{k_{Ex}}{\epsilon^2_{Ex}}+\frac{R_{bl}(1-\sigma_f)}{2\epsilon^2_{bl}}\Big)\|C_{f,p}\|^2_{L^2(\Omega_p)}\\
&\quad+2(\epsilon^2_{Ex}+\epsilon^2_{bl})\|C_{f,bl}\|^2_{L^2(\Omega_p)}+\sum_{i=n,f}\frac{D_v^2E_2^3}{4\epsilon^2_{i,\sigma}\eta}\int_0^t\|\nabla C_{i,p}(s)\|^2_{L^2(\Omega_p)}ds. \qquad (39)
\end{aligned}
$$

Fixing in (39) $\epsilon_{i,j}$ such that $(D_{i,j}-\epsilon^2_{i,j}-\epsilon^2_{i,\sigma})>0$ and $(D^*_{i,p}-\epsilon^2_{i,p}-\epsilon^2_{i,\sigma})>0$ for $i=n,f$ and $j=c,e,r$.

By integrating from (39) and using the Gronwall lemma, we get Theorem 1.

Theorem 1. If $\mathcal{C}=(C_{i,j})$ for $i=n,f,b$ and $j=c,p,e,r,bl$ is a solution of the variational formulation of (3)–(14), respectively, then a positive constant Φ that is independent of time exists such that

$$
\varepsilon(\mathcal{C}(t))\le\frac{1}{\Phi_{\min}}\varepsilon(\mathcal{C}(0))e^{\Phi t}, \qquad (40)
$$

where

$$
\begin{aligned}
\mathcal{C}=&\sum_{\substack{i=n,f\\ j=c,p,e,r,bl}}\|C_{i,j}\|^2_{L^2(\Omega_j)}+\sum_{i=p,bl}\|C_{b,i}\|^2_{L^2(\Omega_p)} \qquad (41)\\
&+\int_0^t\sum_{\substack{i=n,f\\ j=c,p,e,r}}\|\nabla C_{i,j}\|^2_{[L^2(\Omega_j)]^2}ds+\int_0^t\sum_{\substack{i=n,f\\ j=p,e,r}}\|C_{i,j}\|^2_{L^2(\Omega_j)}ds
\end{aligned}
$$

$$+\int_0^t \sum_{i=p,bl} \|C_{b,i}\|^2_{L^2(\Omega_p)} ds + \int_0^t \|C_{f,bl}\|^2_{L^2(\Omega_p)} ds$$
$$+\int_0^t \|C_{f,c}\|^2_{L^2(\Omega_c)} ds + \int_0^t \sum_{\substack{i=c,p \\ j=p,e,r \\ k=n,f}} 2\iota_{i,j} \|[C_{k,i,j}]\|^2_{L^2(\Gamma_{i,j})} ds,$$

$$\Phi = \frac{\Phi_{Max}}{\Phi_{\min}}, \tag{42}$$

$$\begin{aligned}\Phi_{\min} = \min \Big\{ & 1, 2\big(D_{i,j} - \epsilon^2_{i,j} - \epsilon^2_{i,\sigma}\big)_{\substack{i=n,f \\ j=c,e,r}}, 2\big(D^*_{i,p} - \epsilon^2_{i,p} - \epsilon^2_{i,\sigma}\big)_{i=n,f}, \\ & (2\iota_{i,j})_{\substack{i=c,p \\ j=p,e,r}}, 2(k_{rel,p} + R_{ly}), 2k_{rel,e}, 2k_{rel,r}, \\ & 2(k_{rel,bl} + k_{clr,bl}), 2(k_{d,p} + R_{ly} + k_{pb} + k_{Ex}), \\ & 2k_{d,e}, 2k_{d,r}, 2k_{d,c}, 2k_{pu}, \\ & 2(k_{pb} + k_{clr,bl} + k_{Ex} + R_{bl}(1 - \sigma_f))\Big\},\end{aligned}$$

and

$$\begin{aligned}\Phi_{Max} = \max \Big\{ & \Big(\frac{1}{2\epsilon^2_{i,j}} \|\mathbf{v}\|^2_\infty\Big)_{\substack{i=n,f \\ j=c,p,e,r}}, \Big(\frac{k_{rel,i}}{2\epsilon^2_{rel,i}}\Big)_{i=p,e,r}, \Big(\frac{D_v^2 E_2^3}{4\epsilon^2_{i,\sigma}\eta}\Big)_{i=n,f}, \\ & (2\epsilon^2_{rel,i})_{i=p,e,r}, \Big(\frac{k_{pu}}{2\epsilon^2_{pu,i}} + \frac{k_{pb}}{2\epsilon^2_{pb,i}}\Big)_{i=p,bl}, \\ & 2(\epsilon^2_{pu,i} + \epsilon^2_{pb,i})_{i=p,bl}, \Big(\frac{k_{Ex}}{\epsilon^2_{Ex}} + \frac{R_{bl}(1-\sigma_f)}{2\epsilon^2_{bl}}\Big), 2(\epsilon^2_{Ex} + \epsilon^2_{bl})\Big\}.\end{aligned}$$

From Theorem 1, we can conclude that the mathematical model of the problem is stable in a finite time interval. Also, the existence of a solution to weak problem (26)–(37) is a direct consequence of the energy estimate (40).

4.2 Uniqueness of the solution

In this section, we examine the uniqueness of the fully coupled system (fluid flow and drug transport). Two distinct solutions, $(\hat{\mathbf{v}}, \hat{C}_{i,j}, \hat{\sigma})$ and $(\tilde{\mathbf{v}}, \tilde{C}_{i,j}, \tilde{\sigma})$ for $i = n, f, b$ and $j = c, e, p, r, bl$, are examined for (1)–(2), (3)–(6), (9)–(14), (16)–(17) and (18). After subtracting them, use the test functions $\phi_{\mathbf{v}}$, $\phi_{i,j}$ and ϕ_σ to create a weak form. In the equations, enter $\phi_{\mathbf{v}} = w_{\mathbf{v}}$, $\phi_{i,j} = w_{i,j}$

and $\phi_\sigma = w_\sigma$, where $w_{\mathbf{v}} = \hat{\mathbf{v}} - \tilde{\mathbf{v}}$, $w_{i,j} = \hat{C}_{i,j} - \tilde{C}_{i,j}$ and $w_\sigma = \hat{\sigma} - \tilde{\sigma}$, then integrate by part to obtain

$$\begin{aligned}
&\sum_{\substack{i=n,f\\ j=c,p,e,r,bl}} (\frac{\partial w_{i,j}}{\partial t}, w_{i,j}) + 2(\frac{\partial w_\sigma}{\partial t}, w_\sigma) + (\frac{\partial w_{\mathbf{v}}}{\partial t}, w_{\mathbf{v}}) \\
&= - \sum_{\substack{i=n,f\\ j=c,p,e,r}} (D_{i,j}\nabla w_{i,j}, \nabla w_{i,j}) + \sum_{\substack{i=n,f\\ j=c,p,e,r}} (\mathbf{v} w_{i,j}, \nabla w_{i,j}) \\
&\quad + \sum_{\substack{i=n,f\\ j=c,p,e,r}} (w_{\mathbf{v}}\tilde{c}_{i,j}, \nabla w_{i,j}) + \sum_{i=n,f} \big((E_1+E_2)(\frac{\partial w_{i,p}}{\partial t}, w_\sigma) + \frac{E_1E_2}{\eta}(w_{i,p}, w_\sigma)\big) \\
&\quad - \sum_{i=c,e,p,r} k_{d,i}(w_{f,i}, w_{f,i}) - \sum_{i=e,p,r,bl} k_{rel,i}(w_{n,i}, w_{n,i}) - \sum_{i=n,f} R_{ly}(w_{i,p}, w_{i,p}) \\
&\quad - \sum_{i=p,bl} k_{pb}(w_{f,i}, w_{f,i}) - \sum_{i=p,bl} k_{pu}(w_{b,i}, w_{b,i}) - \sum_{i=n,f} k_{clr,i}(w_{i,bl}, w_{i,bl}) \\
&\quad - \sum_{i=p,bl} k_{Ex}(w_{f,i}, w_{f,i}) - R_{bl}(1-\sigma_f)(w_{f,bl}, w_{f,bl}) - \sum_{i=p,e,r,bl} k_{rel,i}\big(w_{n,i}, w_{f,i}\big) \\
&\quad - \sum_{i=p,bl} (k_{pu}+k_{pb})\big(w_{b,i}, w_{f,i}\big) - (2k_{Ex} + R_{bl}(1-\sigma_f))\big(w_{f,p}, w_{f,bl}\big) \\
&\quad -(w_{\mathbf{v}}.\nabla\tilde{\mathbf{v}}, w_{\mathbf{v}}) - \frac{\mu}{\rho}(\nabla w_{\mathbf{v}}, \nabla w_{\mathbf{v}}) - \sum_{i=n,f} D_v(\nabla w_\sigma, \nabla w_{i,p}) - \frac{2E_2}{\eta}(w_\sigma, w_\sigma).
\end{aligned}$$

Using

$$(f,g) \le \frac{1}{2\epsilon}\|f\|^2 + \frac{\epsilon}{2}\|g\|^2,$$

and

$$|\int_\Omega (w_{\mathbf{v}}.\nabla\tilde{\mathbf{v}}) w_{\mathbf{v}} ds| \le \|w_{\mathbf{v}}\|^2_{L^4}\|\nabla\tilde{\mathbf{v}}\|^2_{L^2} \le A\|w_{\mathbf{v}}\|_{L^2}\|\nabla w_{\mathbf{v}}\|_{L^2}\|\nabla\tilde{\mathbf{v}}\|^2_{L^2},$$

we get

$$\begin{aligned}
&\sum_{\substack{i=n,f\\ j=c,p,e,r,bl}} \frac{\partial}{\partial t}\|w_{i,j}\|^2_{L^2(\Omega_j)} + \frac{\partial}{\partial t}\|w_{\mathbf{v}}\|^2_{L^2(\Omega_p)} + 2\frac{\partial}{\partial t}\|w_\sigma\|^2_{L^2(\Omega_p)} \\
&\le \sum_{\substack{i=n,f\\ j=c,e,r}} \big(\epsilon_{i,j} + \epsilon_{v_{i,j}} - 2D_{i,j}\big)\|\nabla w_{i,j}\|^2_{[L^2(\Omega_j)]^2} + \sum_{i=n,f} \epsilon_{1_{i,p}}\|\nabla w_\sigma\|^2 \\
&\quad + \sum_{i=n,f} \big(\epsilon_{i,p} + \epsilon_{v_{i,p}} - 2D_{i,p} + \frac{D_v}{\epsilon_{1_{i,p}}}\big)\|\nabla w_{i,p}\|^2_{[L^2(\Omega_p)]^2} \\
&\quad +(\epsilon_v - \frac{2\mu}{\rho})\|\nabla w_{\mathbf{v}}\|^2_{[L^2(\Omega_j)]^2} - \sum_{i=c,e,p,r} 2k_{d,i}\|w_{f,i}\|^2_{L^2(\Omega_i)}
\end{aligned}$$

$$
\begin{aligned}
&- \sum_{i=e,p,r,bl} 2k_{rel,i}\|w_{n,i}\|^2_{L^2(\Omega_i)} - \sum_{i=n,f} 2R_{ly}\|w_{i,p}\|^2_{L^2(\Omega_p)} \\
&- \sum_{i=p,bl} 2k_{pb}\|w_{f,i}\|^2_{L^2(\Omega_p)} - \sum_{i=p,bl} 2k_{pu}\|w_{b,i}\|^2_{L^2(\Omega_p)} - \sum_{i=n,f} 2k_{clr,i}\|w_{i,bl}\|^2_{L^2(\Omega_p)} \\
&- \sum_{i=p,bl} 2k_{Ex}\|w_{f,i}\|^2_{L^2(\Omega_p)} - 2R_{bl}(1-\sigma_f)\|w_{f,bl}\|^2_{L^2(\Omega_p)} \\
&+ \sum_{\substack{i=n,f \\ j=c,p,e,r}} \big(\frac{1}{\epsilon_{i,j}}\|\mathbf{v}\|^2_{\infty}\|w_{i,j}\|^2_{L^2(\Omega_j)} + \frac{1}{\epsilon_{v_{i,j}}}\|\tilde{C}_{i,j}\|^2\|w_{\mathbf{v}}\|^2\big) \qquad (43) \\
&+ \sum_{i=p,e,r,bl} \frac{k_{rel,i}}{\epsilon_{rel,i}}\|w_{n,i}\|^2_{L^2(\Omega_i)} + \sum_{i=p,e,r,bl} 2\epsilon_{rel,i}\|w_{f,i}\|^2_{L^2(\Omega_i)} \\
&+ \sum_{i=p,bl} \big(\frac{k_{pu}}{\epsilon_{pu,i}} + \frac{k_{pb}}{\epsilon_{pb,i}}\big)\|w_{b,i}\|^2_{L^2(\Omega_p)} + \sum_{i=p,bl} 2(\epsilon_{pu,i}+\epsilon_{pb,i})\|w_{f,i}\|^2_{L^2(\Omega_p)} \\
&+ \frac{2k_{Ex}+R_{bl}(1-\sigma_f)}{\epsilon_{bl}}\|w_{f,p}\|^2_{L^2(\Omega_p)} + 2\epsilon_{bl}\|w_{f,bl}\|^2_{L^2(\Omega_p)} + \frac{A^2}{\epsilon_v}\|w_{\mathbf{v}}\|^2\|\nabla\tilde{\mathbf{v}}\|^2 \\
&+ \sum_{i=n,f} \big(\epsilon_{2_{i,p}}\|\frac{\partial w_{i,p}}{\partial t}\|^2 + \frac{(E_1+E_2)}{\epsilon_{2_{i,p}}}\|w_\sigma\|^2 + \epsilon_{3_{i,p}}\|w_{i,p}\|^2 + \frac{E_1E_2}{\eta\epsilon_{3_{i,p}}}\|w_\sigma\|^2\big)
\end{aligned}
$$

The $\epsilon_i s$ constants can be chosen to be negative $\big(\epsilon_{i,j}+\epsilon_{v_{i,j}}-2D_{i,j}\big)$, $\big(\epsilon_{i,p}+\epsilon_{v_{i,p}}-2D_{i,p}+\frac{D_v}{\epsilon_{1_{i,p}}}\big)$ and $(\epsilon_v - \frac{2\mu}{\rho})$, and the $\epsilon_{1_{i,p}}$ and $\epsilon_{2_{i,p}}$ coefficients can be ignored in (43). Therefor there exists $\alpha \in L^2(0,T)$ such that

$$
\begin{aligned}
&\frac{\partial}{\partial t}\big(\sum_{\substack{i=n,f,b \\ j=c,p,e,r,bl}} \|w_{i,j}\|^2 + \|w_{\mathbf{v}}\|^2 + \|w_\sigma\|^2\big) \\
&\leq \alpha(t)\big(\sum_{\substack{i=n,f,b \\ j=c,p,e,r,bl}} \|w_{i,j}\|^2 + \|w_{\mathbf{v}}\|^2 r + \|w_\sigma\|^2\big).
\end{aligned}
$$

In other words, $\|w_{\mathbf{v}}\|$, $\|w_\sigma\|$ and $\|w_{i,j}\|$ $i = n, f, b$ $j = c, p, e, r, bl$ are obviously zero at $= 0$. We can thus prove the uniqueness of the solution by applying the Gronwall lemma, which yields $\|w_{\mathbf{v}}\|^2 = \|w_\sigma\|^2 = \|w_{i,j}\|^2 = 0$ $i = n, f, b$ $j = c, p, e, r, bl$.

5 Numerical simulations

5.1 Numerical methods and independence of the solution on the mesh

Equations (1)–(21) were solved in the geometry shown in Figure 1b. The numerical results presented in what follows are obtained using COMSOL Multiphysics 5.6. The piecewise linear finite element space P_1 is used for the concentration and P_2 for flow equations, and the backward differential formula with order between 1 and 2 with time step length 0.01 is used to take the integral in time. A triangular mesh was created automatically. Table 2 provides the values used for the parameters in the numerical simulation.

Table 2: Values of the parameters for drug properties.

Parameter and Symbol	Values	Units	Reference
Diffusivity in CH($D_{f,c}, D_{n,c}$)	3.8×10^{-10}	m^2/s	[5, 35]
Diffusivity in skin tissues ($D_{i,j}$ $i = n, f$ $j = e, p, r, bl$)	1×10^{-10}	m^2/s	[5, 23]
Density(ρ)	1000	kg/m^3	[5]
Drug degradation rate(k_d)	5.6×10^{-6}	$1/s$	[5, 33]
Drug release rate(k_{rel})	1×10^{-4}	$1/s$	[5]
Drug association rate with protein(k_{pb})	0.833	$1/s$	[5, 10]
Drug dissociation rate from protein(k_{pu})	0.278	$1/s$	[5, 10]
Constant dependent(k_{Ex})	2.3×10^{-3}	$1/s$	[5]
Rate of fluid exchange(R_{ly})	4.2×10^{-7}	$1/s$	[5]
Rate of fluid exchange(R_{bl})	1.19×10^{-5}	$1/s$	[5]
Rate of plasma clearance(k_{clr})	5×10^{-5}	$1/s$	[5, 23]
Osmotic reflection coefficient of drug(σ_f)	0.15		[5]
Viscosity(μ)	0.78	$Pa.s$	[5]
Stiffness coefficient of the single spring(E_1)	1.2294×10^{-1}	Pa	[4, 15]
Stiffness coefficient of the spring(E_2)	1.7239×10^{-1}	Pa	[4, 15]
Stiffness coefficient of the dashpot(η)	1.0532×10^{-1}	$N/m.s$	[4, 15]
Viscoelastic diffusion coefficient(D_v)	5×10^{-12}	$mol/m^3.s.Pa$	[4, 15]

The various meshes are taken into consideration to ensure that the numerical results are independent of the mesh size. Using convergence tests, the mesh density's adequacy has been examined. For two different meshes, the convergence of the solutions and the mesh independence have been investigated. To better demonstrate this assertion, Figure 2 and Tables 3 and 4 compare various meshes for the average concentrations of nanocarriers and free drug in the PD, respectively. Notably, the reference solution is defined by a mesh consisting of 1702 elements. Figure 2 indicates that the numerical results are independent of mesh size, as the changes between the meshes are nearly indistinguishable.

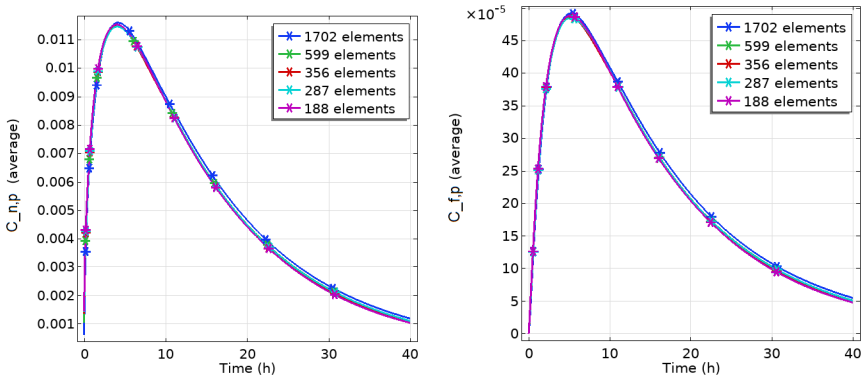

(a) (b)

Figure 2: Average nanocarrier concentrations (a) and free drug concentrations (b) in the PD to demonstrate that numerical results are independent of meshing.

Table 3: Different errors for nanocarriers concentration in PD.

Number of elements	L^∞-norm	L^2-norm
599	4.26×10^{-4}	1.10×10^{-2}
356	9.34×10^{-4}	1.83×10^{-2}
287	9.73×10^{-4}	1.95×10^{-2}
188	1.03×10^{-3}	1.96×10^{-2}

Table 4: Different errors for free drug concentration in PD.

Number of elements	L^∞-norm	L^2-norm
599	1.09×10^{-5}	4.65×10^{-4}
356	1.65×10^{-5}	7.82×10^{-4}
287	1.73×10^{-5}	8.40×10^{-4}
188	1.76×10^{-5}	8.45×10^{-4}

Figure 3a shows a flow velocity diagram in CH, with arrows indicating the flow direction. The average free drug concentrations in CH, PD and BL, computed with and without convective transport, are plotted in Figure 3b,3c, and 3d to show how convection affects drug transport in various domains. Convection has an increasing impact on drug transport, according to these plots.

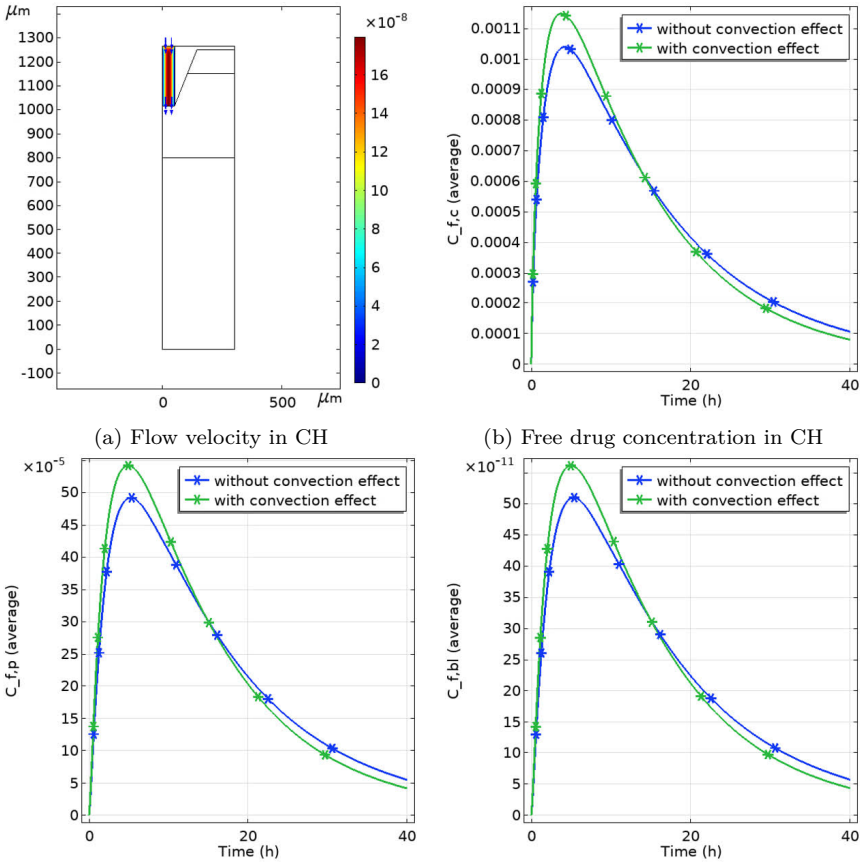

(a) Flow velocity in CH

(b) Free drug concentration in CH

(c) Free drug concentration in PD

(d) Free drug concentration in BL

Figure 3: Effect of flow velocity on the drug transport

5.2 Convergence study

In what follows, we assume that the domains of $\Omega_i, i = c, e, p, r$ are polygonal lines. Suppose that $\Im_{i,h}, i = c, e, p, r, h \to 0$ is a sequence of admissible triangles from $\Omega_i, i = c, e, p, r$, respectively, with $\max_{\triangle \in \Im_{i,h}} diam(\triangle) \to 0$. We assume that the triangles on the common boundary are

congruent. By $V_{i,h}$ we denote the subspace $H^1(\Omega_i)$ defined by the piecewise linear functions of u_h induced by the triangulation of $\Im_{i,h}$ for $i = c, e, p, r$. Let $C_{i,j,h} \in \prod V_{k,h}$ for $i = n, f, b$, $j = c, e, p, r, bl$ and $k = c, e, p, r$ be the approximate piecewise linear solutions of (3)–(6), (9)–(14) and (16)–(17). Then, considering $e_{i,j} = C_{i,j} - C_{i,j,h}$ for $i = n, f, b$, $j = c, e, p, r, bl$ and following the procedure for proving in section 4.2, we get the following results:

$$\begin{aligned}
&\frac{d}{dt}\Big(\sum_{\substack{i=n,f\\ j=c,p,e,r,bl}} \|e_{i,j}\|^2_{L^2(\Omega_j)} + \sum_{j=p,bl} \|e_{b,j}\|^2_{L^2(\Omega_p)}\Big)\\
&+ \sum_{\substack{i=n,f\\ j=c,e,r,p}} 2\big(D_{i,j} - \epsilon^2_{i,j,1} - \epsilon^2_{i,j,2}\big)\|\nabla e_{i,j}\|^2_{[L^2(\Omega_j)]^2}\\
&\quad\le \sum_{\substack{i=n,f\\ j=c,e,r,p}} \big(\frac{1}{2\epsilon^2_{i,j,1}}\|\mathbf{v}_h\|^2_\infty + A_{i,j}\big)\|e_{i,j}\|^2\\
&\qquad + \sum_{\substack{i=n,f\\ j=c,e,r,p}} \frac{1}{2\epsilon^2_{i,j,2}}\|e_{\mathbf{v}}\|^2_\infty\|c_{i,j}\|^2_\infty + \big(\frac{D_v}{2\epsilon^2_{n,p,3}} + \frac{D_v}{2\epsilon^2_{f,p,6}}\big)\|\nabla e_\sigma\|_{[L^2(\Omega_p)]^2}
\end{aligned} \tag{44}$$

where $A_{f,c} = -2k_{d,c}$, $A_{n,e} = \frac{k_{rel,e}}{2\epsilon^2_{f,e,3}} - 2k_{rel,e}$, $A_{f,e} = 2\epsilon^2_{f,e,3} - 2k_{d,e}$,
$A_{b,p} = \frac{k_{pu}}{2\epsilon^2_{f,p,3}} - 2k_{pu}$, $A_{n,r} = \frac{k_{rel,r}}{2\epsilon^2_{f,r,3}} - 2k_{rel,r}$, $A_{f,r} = 2\epsilon^2_{f,r,3} - 2k_{d,r}$,
$A_{n,bl} = \frac{k_{rel,bl}}{2\epsilon^2_{f,bl}} - 2k_{rel,bl} - 2k_{clr,n}$, $A_{b,bl} = \frac{k_{pu}}{2\epsilon^2_{f,bl,2}} + 2\epsilon^2_{b,bl} - 2k_{pu}$,
$A_{n,p} = \frac{k_{rel,p}}{2\epsilon^2_{f,p,4}} + 2\epsilon^2_{n,p,3} - 2R_{ly} - 2k_{rel,p}$,
$A_{f,p} = \frac{k_{Ex}}{2\epsilon^2_{f,bl,3}} + 2\epsilon^2_{f,p,3} + 2\epsilon^2_{f,p,4} + 2\epsilon^2_{f,p,5} + 2\epsilon^2_{f,p,6} - 2R_{ly} - 2k_{Ex} - 2k_{d,p} - 2k_{pb}$,
$A_{f,bl} = \frac{k_{pb}}{2\epsilon^2_{f,bl}} + \frac{(k_{Ex}+R_{bl}(1-\sigma_f))}{2\epsilon^2_{f,p,5}} + 2\epsilon^2_{f,bl,2} + 2\epsilon^2_{f,bl} + 2\epsilon^2_{b,bl,3} - 2k_{Ex} - 2k_{pb} - 2k_{clr,f} - 2R_{bl}(1-\sigma_f)$.

Put $g(\mathbf{v}_h(t)) = \big(\frac{1}{2\epsilon^2_{i,j,1}}\|\mathbf{v}_h\|^2_\infty + A_{i,j}\big)$, then inequality (44) leads to

$$\begin{aligned}
&\sum_{\substack{i=n,f\\ j=c,p,e,r,bl}} \|e_{i,j}\|^2_{L^2(\Omega_j)} + \sum_{j=p,bl} \|e_{b,j}\|^2_{L^2(\Omega_p)}\\
&+ \int_0^t e^{\int_s^t g(\mathbf{v}_h(\mu))d\mu} \sum_{\substack{i=n,f\\ j=c,e,r,p}} 2\big(D_{i,j} - \epsilon^2_{i,j,1} - \epsilon^2_{i,j,2}\big)\|\nabla e_{i,j}\|^2_{[L^2(\Omega_j)]^2} ds\\
&\quad\le e^{\int_s^t g(\mathbf{v}_h(\mu))d\mu}\Big(\sum_{\substack{i=n,f\\ j=c,p,e,r,bl}} \|e_{i,j}(0)\|^2_{L^2(\Omega_j)} + \sum_{j=p,bl} \|e_{b,j}(0)\|^2_{L^2(\Omega_p)}\Big)\\
&\qquad + \int_0^t e^{\int_s^t g(\mathbf{v}_h(\mu))d\mu}\Big(\sum_{\substack{i=n,f\\ j=c,e,r,p}} \frac{1}{2\epsilon^2_{i,j,2}}\|e_{\mathbf{v}}\|^2_\infty\|c_{i,j}\|^2_\infty
\end{aligned}$$

$$+\Big(\frac{D_v}{2\epsilon_{n,p,3}^2}+\frac{D_v}{2\epsilon_{f,p,6}^2}\Big)\|\nabla e_\sigma\|^2_{[L^2(\Omega_p)]}\Big)ds.$$

The following conclusion can be reached by using the approximation that was employed in [14, 16].

$$\sum_{\substack{i=n,f\\ j=c,p,e,r,bl}}\|e_{i,j}\|^2_{L^2(\Omega_j)}+\sum_{j=p,bl}\|e_{b,j}\|^2_{L^2(\Omega_p)}+\int_0^t\sum_{\substack{i=n,f\\ j=c,p,e,r,bl}}\|\nabla e_{i,j}\|^2ds\leq\mathbb{C}h^4,$$

where $\mathbb{C}$ is the positive constant that is independent of h and t.

5.3 Numerical simulations and sensitive analysis

Figures 4a and 4b show the concentration of nanocarrier in the circulatory system and skin tissues and how that concentration changes over time. The findings indicate a gradual decrease in this concentration after it first rises in all skin components. The PD has a higher concentration than the VE and RD, respectively, because the needle is located there. The last location of this drug delivery process is the circulatory system, which has the lowest concentration. It is clear from the figure that at the beginning of diffusion, an immediate jump in concentration occurs inside the PD compared to the VE and RD. As shown in Figure 4c, the concentration of free drug is displayed along the skin layers. It is evident, nevertheless, that most of the drug is present in the skin layers as bound drug. Figure 4d illustrates the percentage of the drug that enters the bloodstream as both bound and free.

Figures 5 and 6 demonstrate the impact of drug release rate on drug delivery outcomes in skin and blood. It is evident that quick drug release can successfully lower the amount of nanocarriers in BL and all skin layers (Figure 5). In contrast, the concentration of free drug varies. Because nanocarriers penetrate the PD, an increased rate of release enables the drug to diffuse more quickly, which raises the concentration of free drug quickly. However, more free drug can be moved from the PD to the VE and RD due to faster release.

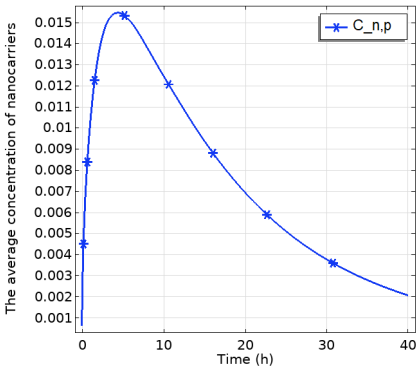

(a) The concentration of nanocarriers in PD

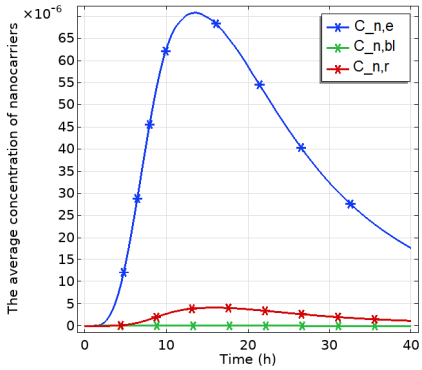

(b) The concentration of nanocarriers in VE, RD, BL

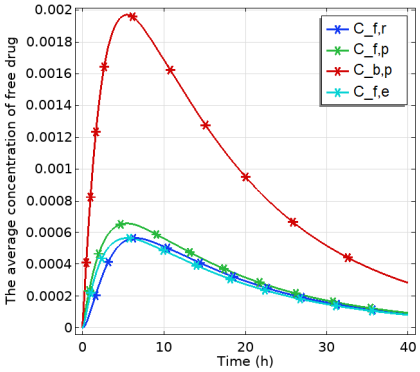

(c) The concentration of released drugs in skin

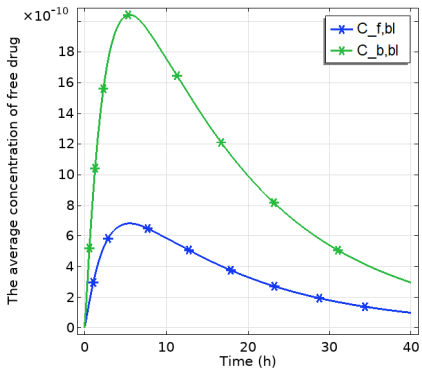

(d) The concentration of released drugs in blood

Figure 4: Drug concentrations in blood and skin tissues over time.

5.4 Dependence on viscoelastic properties and comparing the model

In the previous sections, we assumed a constant value for the viscoelastic diffusion coefficient. In this section, we want to analyze the dependence of the concentrations of the nanocarrier and free drug on D_v. Figure 7 illustrates how the viscoelastic diffusion coefficient D_v affects the release of the nanocarrier and, consequently, the free drug in PD and BL. As the figures demonstrate, we can anticipate less nanocarrier accumulation and, as a result, less free drug accumulation in PD and BL as D_v rises. This is due to the fact that the elastin present in the dermis increases the resistance of the dermis to the entry of the drug through the MN CH. Ultimately, the amount of drug that enters the bloodstream decreases as the viscoelastic diffusion coefficient increases. This important property was not mentioned in [5].

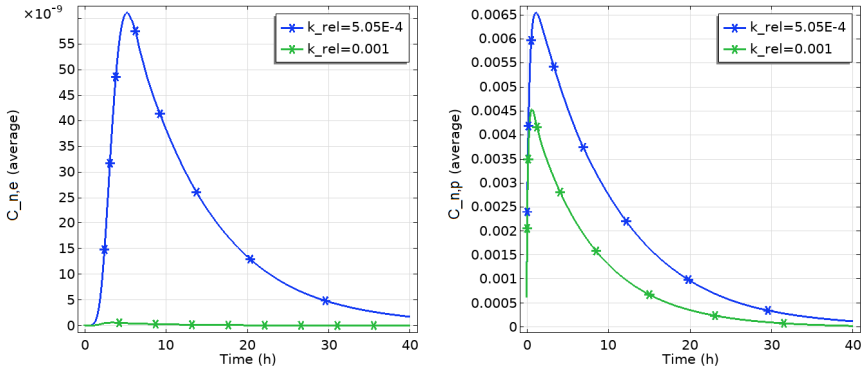

(a) Nanocarriers concentration in VE (b) Nnocarriers concentration in PD

(c) Nanocarriers concentration in RD (d) Nanocarriers concentration in BL

Figure 5: The effect of drug release rate (k_{rel}) on the nanocarriers concentration in skin and BL.

The comparison between the model presented in this paper and Benbrook and Zhan's model presented in [5] is illustrated in Figure 8 and Table 5. Figure 8 shows the average concentration of the drug in the bloodstream. This figure illustrates how the viscoelastic term, which was added to our model to reflect the skin's viscoelastic property, which acts as a barrier, causes the concentration of nanocarriers and free drug to be lower than those in Zhan's model. Table 5 shows a quantitative comparison of nanocarrier and free drug concentrations in PD and BL between our model and Zhan's model. These values were recorded at a set time of 20 hours. From this table, it is clear that the viscoelastic property affects the transport of drugs and acts as a barrier to drug delivery.

To confirm our work and the effectiveness of the model, the results of this model were compared in Figure 9a with the experimental results in [9]. As can be seen, our results are in line with experimental results demonstrating that the model is valid. The viscoelasticity of the skin degrades as a result of diseases and hydration loss brought on by aging [11]. According to

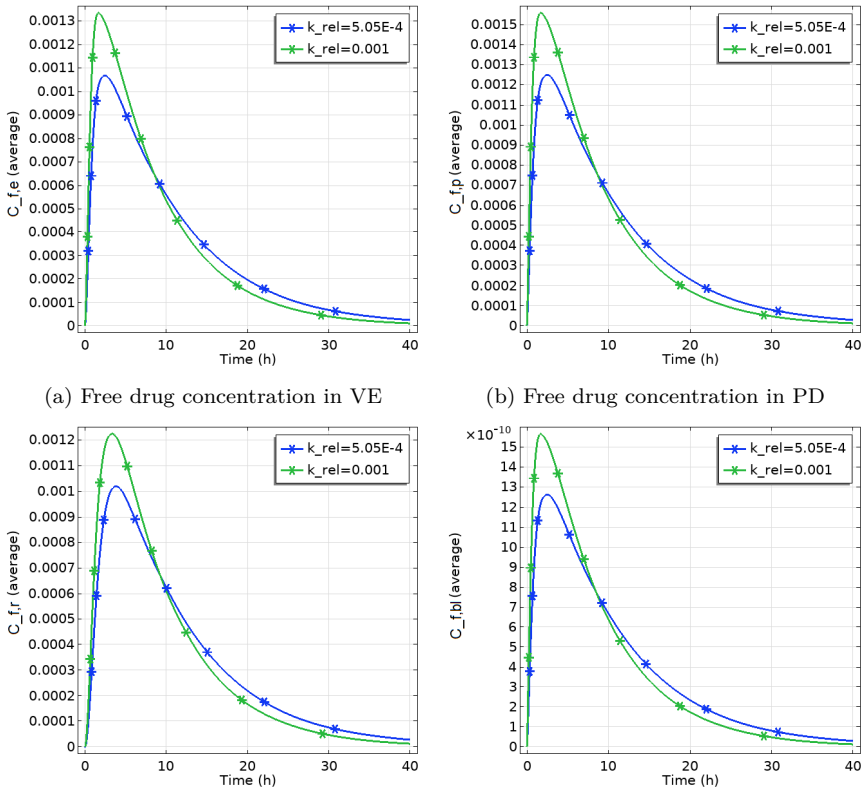

(a) Free drug concentration in VE

(b) Free drug concentration in PD

(c) Free drug concentration in RD

(d) Free drug concentration in BL

Figure 6: The effect of drug release rate (k_{rel}) on the free drug concentration in skin and BL.

[8], which explores how age affects the viscoelastic properties of the skin, three important and influential factors are reduced with age: the immediate contraction of the skin after release of negative pressure, the total contraction after the first cycle, and the ratio of the instantaneous contraction to the maximum deformation, which measures the skin's biological elasticity. This results in a reduction of stiffness in the Zener model. This paper shows that, on average, the parameters decline by 0.6 units between 20 and 60 years of age. To illustrate how drug delivery changes with age, we consider in Figure 9b two different values of stiffness and observe that viscoelastic skin properties decrease with age, leading to increased drug delivery into the skin.

Table 5: Quantitative comparison of our model with Zhan's model at a set time of 20 hours.

	$C_{n,p}$	$C_{f,p}$	$C_{n,bl}$	$C_{f,bl}$
Benbrook and Zhan's model [5]:	0.0069526	3.1846×10^{-4}	3.1249×10^{-8}	3.3212×10^{-10}
Our model:	0.0046546	2.1459×10^{-4}	2.1340×10^{-8}	2.2393×10^{-10}

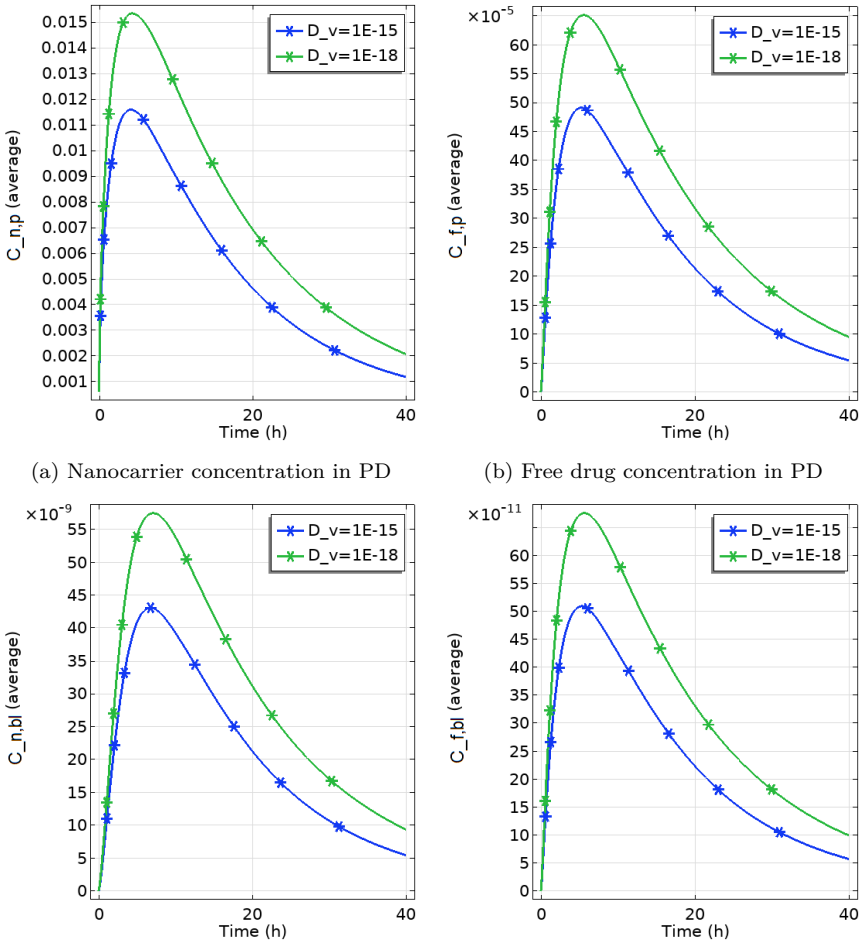

(a) Nanocarrier concentration in PD

(b) Free drug concentration in PD

(c) Nanocarrier concentration in BL

(d) Free drug concentration in BL

Figure 7: The impact of the viscoelastic diffusion coefficient (D_v) on the various PD concentrations.

6 Conclusion

A mathematical model incorporating ordinary and partial equations, along with initial and boundary conditions, has been developed to analyze the transport of nanocarriers and drugs via a hollow MN embedded in the skin. It describes drug diffusion into the nanocarrier, free drug, and bound drug states. The objective is to facilitate drug entry into the bloodstream using a nanocarrier positioned in the MN CH. This model accounts for the skin's mechanical characteristics influenced by elastin in the dermis and demonstrates significant effects on drug delivery through numerical results. Some conclusions from this analytical and numerical study are presented.

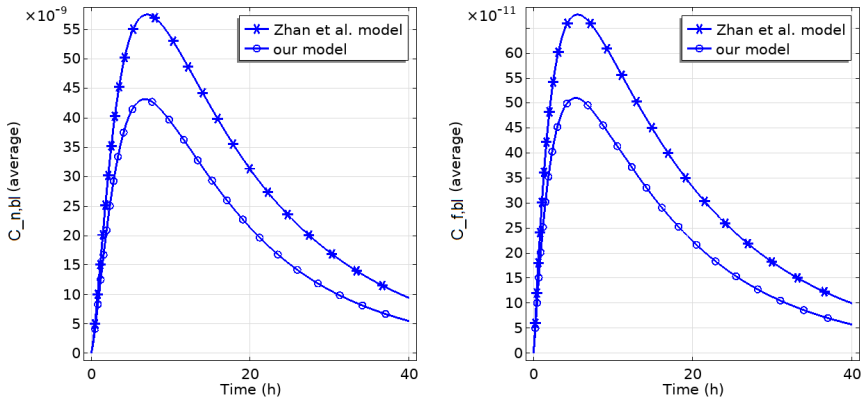

(a) (b)

Figure 8: Comparison of the nanocarriers concentration (a) and the free drugs concentration (b) in BL in our model with the model presented in [5].

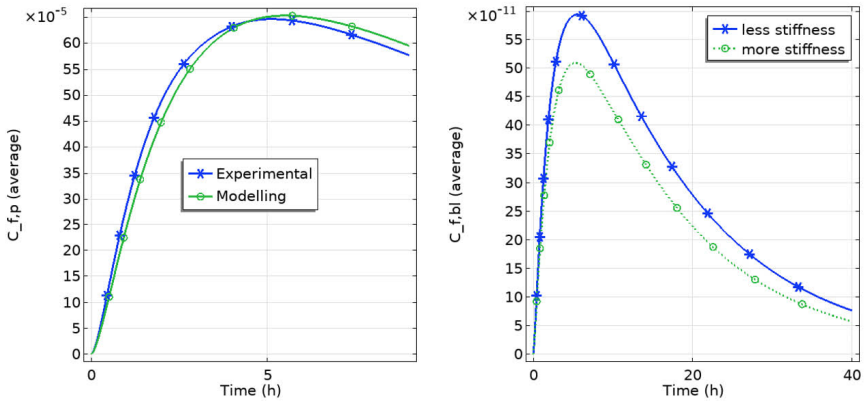

(a) (b)

Figure 9: Model validation. (a) Comparison of model predicted free drug concentration in PD with laboratory measurements. (b) Effect of age, disease state and skin hydration on viscoelastic properties.

- Using energy estimation, the stability of the model solution and its uniqueness can be proven (Theorem 1);
- By taking into account various meshes and comparing the convergence of solutions using the L^2 and L^∞ norms, it is possible to determine the independence of numerical results from mesh size (Figure 2 and Tables 3 and 4);
- Considering the viscoelasticity of the skin due to the presence of elastin in the dermis, we see that it has a significant effect on drug transport. As shown in Figure 7, less drug enters the PD and, eventually, less drug enters the bloodstream as D_v rises (Figure 7);

- The negative effect of the skin properties as a result of diseases and hydration loss brought on by aging on viscoelasticity and thus on drug delivery to skin was investigated (Figure 9b);

- Comparing our model with the model presented by [5] (Figure 8), this difference value is related to considering the viscoelastic effect on the skin (Equations (16) and (17)).

As a future work, we plan to consider the three-dimensional model in real terms so that we can get closer to reality.

Declarations

Conflict of interest There is no conflicting of interest.

Funding

This research received no external funding.

Conflicts of Interest

All authors jointly worked on the results and they read and approved the final manuscript, and also declare that they have no competing interests.

References

[1] Abdo, J.M., Sopko, N.A. and Milner, S.M. *The applied anatomy of human skin: A model for regeneration*. Wound Med., 28 (2020), 100179.

[2] Anissimov, Y.G. and Roberts, M.S. *Modelling dermal drug distribution after topical application in human*. Pharm Res., 28 (2011), 2119–2129.

[3] Azhdari, E. and Emami, A. *Swelling effect of microneedle in the skin drug delivery using Stephan condition: Analytical and numerical study*. Ric. Mat., (2024), 1–28.

[4] Azhdari, E. and Naghipoor, J. *The effect of viscoelasticity of the tissue on the magneto-responsive drug delivery system*. J. Math. Biol., 84(13) (2022), 1–26.

[5] Benbrook, N. and Zhan, W. *Mathematical modelling of hollow microneedle-mediated transdermal drug delivery*. Drug Deliv. Transl. Res., 15 (2025). 3226–3251.

[6] Calcutt, J.J., Roberts, M.S. and Anissimov, Y.G. *Predicting viable skin concentration: Modelling the subpapillary plexus*. Pharm Res., 39 (2022), 783–793.

[7] Cárcamo-Martínez, Á., Mallon, B., Domínguez-Robles, J., Vora, L.K., Anjani, Q.K. and Donnelly, R.F. *Hollow microneedles: A perspective in biomedical applications*. Int. J. Pharm., 599 (2021), 120455.

[8] Chen, D., Yin, S., Lu, X., Fu, H., Gao, H. and Zhang, S. *Research on the correlation between skin elasticity evaluation parameters and age*. Cosmetics, 11(6) (2024), 205.

[9] Davis, S.P., Martanto, W., Allen, M.G. and Prausnitz, M.R. *Hollow metal microneedles for insulin delivery to diabetic rats*. IEEE Trans. Biomed. Eng., 52 (2005), 909–915.

[10] Eikenberry, S. *A tumor cord model for Doxorubicin delivery and dose optimization in solid tumors*. Theor. Biol. Med. Model., 6 (2009), 16.

[11] Everett, J.S. and Sommers, M.S. *Skin viscoelasticity: Physiologic mechanisms, measurement issues, and application to nursing science*. Biol. Res. Nurs., 15(3) (2013), 338–346.

[12] Ferreira, J.A., Grassi, M., Gudino, E. and de Oliveira, P. *A 3d model for mechanistic control drug release*. SIAM J. Appl. Math., 74 (2014), 620–633.

[13] Ferreira, J.A., Grassi, M., Gudiuo, E. and de Oliveira, P. *A new look to non-fickian diffusion*. Appl. Math. Model., 39 (1) (2015), 194–204.

[14] Ferreira, J.A., Jordão, D. and Pinto, L. *Drug delivery enhanced by ultrasound: Mathematical modeling and simulation*. Comput. Math. Appl., 107 (2022), 57–69.

[15] Ferreira, J.A., Naghipoor, J. and de Oliveira, P. *A coupled non-fickian model of a cardiovascular drug delivery system*. Math. Med. Biol., 33(3) (2016), 329–357.

[16] Ferreira, J.A., Pinto, L. and Santos, R. *Numerical analysis of a porous-elastic model for convection enhanced drug delivery*. J. Comput. Appl. Math., 339 (2022), 113719.

[17] Goyal, R., Macri, L.K., Kaplan, H.M. and Kohn, J. *Nanoparticles and nanofibers for topical drug delivery*. J. Control Release, 240 (2016), 77–92.

[18] Jacquet, E., Chambert, J., Pauchot, J. and Sandoz, P. *Intra-and inter-individual variability in the mechanical properties of the human skin from in vivo measurements on 20 volunteers*. Skin Res. Technol., 23 (2017), 491–499.

[19] Lee, H., Song, C., Baik, S., Kim, D., Hyeon, T. and Kim, D-H. *Deviceassisted transdermal drug delivery*. Adv. Drug Deliv. Rev., 45 (2018), 127–135.

[20] Li, M., Vora, L.K., Peng, K. and Donnelly, R.F. *Trilayer microneedle array assisted transdermal and intradermal delivery of dexamethasone*. Int. J. Pharm., 612 (2022), 121295.

[21] Lotfollahi, Z. *The anatomy, physiology and function of all skin layers and the impact of ageing on the skin*. Wound Pract. Res., 32(1) (2024), 6–10.

[22] Machekposhti, S.A., Soltani, M., Najafizadeh, P., Ebrahimi, S.A. and Chen, P. *Biocompatible polymer microneedle for topical/dermal delivery of tranexamic acid*. J. Control Release, 261 (2017), 87–92.

[23] McLean, K. and Zhan, W. *Mathematical modelling of nanoparticle-mediated topical drug delivery to skin tissue*. Int. J. Pharm., 611 (2022), 121322.

[24] Muliana, A. and Rajagopal, K.R. *Modeling the response of nonlinear viscoelastic biodegradable polymeric stents*. Int. J. Solids Struct., 49 (2012), 989–1000.

[25] Nekouzadeh, A., Pryse, K.M., Elson, E.L. and Genin, G.M. *A simplified approach to quasilinear viscoelastic modeling*. J. Biomech., 40 (2007), 3070–3078.

[26] Palacio-Torralba, J., Hammer, S., Good, D.W., McNeill, S.A., Stewart, G.D., Reuben, R.L. and Chen, Y. *Quantitative diagnostics of soft tissue through viscoelastic characterization using time-based instrumented palpation*. J. Mech. Behav. Biomed. Mater., 41 (2015), 149–160.

[27] Phatale, V., Vaiphei, K.K., Jha, S., Patil, D., Agrawal, M. and Alexander, A. *Overcoming skin barriers through advanced transdermal drug delivery approaches*. J. Control Release, 80 (2022), 351–361.

[28] Prausnitz, M.R., Mitragotri, S. and Langer, R. *Current status and future potential of transdermal drug delivery*. Nat. Rev. Drug Discov., 3 (2004), 115–124.

[29] Prausnitz, M.R. and Langer, R. *Transdermal drug delivery*. Nat. Biotechnol., 26 (2008), 1261–1268.

[30] Rippa, A.L., Kalabusheva, E.P. and Vorotelyak, E.A. *Regeneration of dermis: Scarring and cells involved*. Cells, 8(6) (2019), 607.

[31] Soares, J.S. and Zunino, P. *A mixture model for water uptake, degradation, erosion and drug release from polydisperse polymeric networks*. Biomaterials, 31 (2010), 3032–3042.

[32] Wu, Y., Hutton, A.R.J., Pandya, A.K., Patravale, V.B. and Donnelly, R.F. *Microneedle and polymeric films: Delivery of proteins, peptides and nucleic acids*. Drug Deliv. Target., (2023), 93–111.

[33] Wu, D.C. and Ofner, C.M. *Adsorption and degradation of doxorubicin from aqueous solution in polypropylene containers*. AAPS PharmSciTech, 14 (2013), 74–77.

[34] Yadav, P.R., Munni, M.N., Campbell, L., Mostofa, G., Dobson, L., Shittu, M., Pattanayek, S.K., Uddin, v. and Das, v. *Translation of polymeric microneedles for treatment of human diseases: Recent trends, progress, and challenges*. J. Math. Biol., 84(8) (2021), 1132.

[35] Zhan, W. *Mathematical modelling of drug delivery to solid tumour*. Imperial College London, 2014.